2011 American Control Conference
on O'Farrell Street, San Francisco, CA, USA
June 29 - July 01, 2011

Modeling the Effect of Temozolomide Treatment on Orthotopic Models of Glioma

Francisco G. Vital-Lopez, Costas D. Maranas, and Antonios Armaou, *Member, IEEE*

Abstract— **We present a hybrid cellular-tumor level model of brain tumor progression. The model describes tumor progression as the collective outcome of individual tumor cells, the behavior of which is governed by the interplay of intracellular signaling pathways (i.e., MAPK pathway) and the spatial-temporal distribution of key biochemical cues (e.g., oxygen, growth factors). The model is deployed to simulate the effect of different schedule-dose combinations of a chemotherapeutic agent (i.e., temozolomide) on tumor growth in murine orthotopic models of glioma. Simulation results are in good quantitative agreement with experimental measurements. In addition, the model is used to predict the outcome of alternative treatment strategies. Model simulations can be helpful for designing more efficient treatment strategies.**

I. Introduction

Primary brain tumors are a varied group of intracranial neoplasms originating from different tissues of the central nervous system with different degrees of malignancy. The most common of these tumors are the gliomas, which account for nearly 50% of all cases [1]. A type of glioma, known as glioblastoma multiforme or just glioblastoma, is the most frequent and lethal of the brain tumors [2] and it is estimated that represents approximately 80% of the malignant brain tumors [3]. Glioblastomas are characterized by a high rate of uncontrolled proliferation. In general they exhibit necrotic regions, marked angiogenesis, asymmetrical infiltrating invasiveness and they are highly refractory to radio/chemotherapy.

Current glioblastoma treatments include supportive care to alleviate symptoms of the disease (e.g., cerebral edema, seizures, cognitive dysfunctions, etc.) and local and/or systemic therapies to ablate the tumor. Anti-tumor therapies traditionally involve surgical resection followed by radiotherapy and chemotherapy. However, almost all glioblastoma patients relapse after initial therapy and the median overall survival is about 15 months, only modestly improving over the last 25 years [4].

Temozolomide (TMZ) is a cytotoxic drug approved by the FDA for the treatment of anaplastic astrocytoma and glioblastoma [5]. Clinical trials documented a statistically significant survival benefit of the use of temozolomide in combination with radiotherapy for the treatment of newly diagnosed glioblastomas [6]. However, the emergence of various resistant mechanisms have limited the efficacy in the management of high-grade gliomas. This has motivated a number of studies to increase the efficacy of the treatment. These studies reported that the efficacy of TMZ is highly schedule-dose dependent [7].

A major factor in treatment failure is the diffuse infiltration of highly invasive tumor cells into the surrounding tissue from the early stages of tumor development, generally resulting in recurrence just a few months after surgery [4, 8]. This has stirred considerable efforts to elucidate the underlying mechanisms of the perivascular migration of cancer cells at the molecular [9, 10], cellular [11, 12] and tumor [13] levels. These studies have provided important insights about the tumor cell invasion process. However, the decryption of tumor invasiveness is still ongoing and it requires that tumor cell migration be investigated in concert with other biological processes such as cellular proliferation, necrosis, host vessel co-option and angiogenesis, and external factors such as treatments.

Mathematical modeling of tumor progression has been an active area over the last years. A large number of models have been published with focus on varied aspects of the tumor progression and with different levels of detail. Some models consider only tumor growth while others incorporate other processes such as angiogenesis or the effect of a therapeutic agent. From the mathematical point of view, models can be classified according to the modeling approach they deploy. Two major categories are continuum based and discrete based models whereas their combination gives rise to an important third category of hybrid continuum-discrete models. A comprehensive review of the abundant literature in this field is out of the scope of this work. The reader may refer to reviews focused on modeling of tumor growth [14-16], continuum based models [17], discrete based models [18], tumor-induced angiogenesis[19-22] , tumor therapy [23] and brain tumors [24-28] for more information.

In this work, we develop a hybrid multi-scale agent based model to simulate the progression of a brain tumor (i.e., glioblastoma). We describe tumor progression as the outcome of the evolution in space and time of a collection of tumor cells that dynamically interact with their environment. The model integrates the dynamics of key biological processes occurring at the cellular and tumor levels. We deploy the model to investigate the effect of temozolomide

Manuscript received September 27, 2010. This work was supported in part by the Penn State Institute for CyberScience Seed Funding and the National Science Foundation (NSF-CAREER award #CBET 06-44519).

A. Armaou is with The Pennsylvania State University, University Park, PA 16802 USA (corresponding author; phone: 814-865-5316; fax: 814-865-7846; e-mail: armaou@ engr.psu.edu).

F. G. Vital-Lopez is with The Pennsylvania State University, University Park, PA 16802 USA (e-mail: fvitallopez@engr.psu.edu).

C. D. Maranas is with The Pennsylvania State University, University Park, PA 16802 USA (e-mail: costas@engr.psu.edu).

(a chemotherapeutic agent) dosing and scheduling in the progression of the tumor. First we validate the model against data from experiments with orthotopic models of glioma [7] and then we use the model to predict the outcome of alternative therapeutic strategies.

II. Model Description

The model consists of two interdependent components, which describe processes at the cellular and tumor levels, shown pictorially in Fig. 1. At the cellular level, the state of individual tumor cells is governed by a set of rules depending on their local environment (i.e., concentrations of oxygen, VEGF, and TGFα) and intracellular signaling pathways (i.e., MAPK signaling pathway). The tumor level component determines the spatio-temporal distribution of the key biochemical cues. The two components are connected through the interchange of information required to solve the whole model. Specifically, the local concentration of biochemical cues for every tumor cell is obtained from the solution of the tumor level component whereas the production and consumption terms for the tumor level component are determined by cellular level component.

A. Tumor level model component

The tumor level model captures the spatio-temporal distribution of extracellular species and tumor cells within the simulation domain. The profiles of the chemical species are described by a set of PDEs. Tumor cells are treated as discrete entities (i.e., agents). We follow a lattice-free approach to determine the location of the tumor cells. The simulation domain (Ω) is a cubic region of the white matter of dimension 12×12×12 mm^3, which is chosen large enough to minimize the effect of the boundary conditions on chemical species concentrations. During the simulations, we record the spatio-temporal distribution of oxygen, TGFα, VEGF, and temozolomide as well as the state of every tumor cell. The state of each tumor cell is defined by its phenotype, location, cellular mass and the activation level of its MAPK pathway (i.e., phosphorylation level of ERK (ERK_{act})).

The concentration of extracellular species is considered to be continuous fields described by a set of PDEs:

$$D_i\nabla^2 C_i + K_T^i(z)(C_{i,v} - C_i) + S_i(z, C_{intra}) - k_i(z)C_i = 0, \quad C_i \in \Omega, \tag{1}$$

with boundary conditions:

$$\mathbf{n}\cdot(D_i\nabla C_i) = 0, \quad C_i \in \Gamma, \tag{2}$$

where for species i, C_i is its extracellular concentration, D_i is its diffusion coefficient, K_T^i is its supply rate from the blood vessels, and k_i is its consumption rate constant (assuming first order process for all the species). The source term $S_i(\cdot)$ refers to the production of TGFα and VEGF by tumor cells and depends on the activation level of the MAPK pathway and the metabolic state of the tumor cells at the location z. Ω is defined as the computational domain of the PDEs and Γ is the boundary of Ω while $\mathbf{n}$ is the normal vector to Γ. No-flux boundary conditions are assumed. The parameters of the tumor level model are collected from the open literature when available or estimated to approximate reported levels in the brain of the chemical species considered.

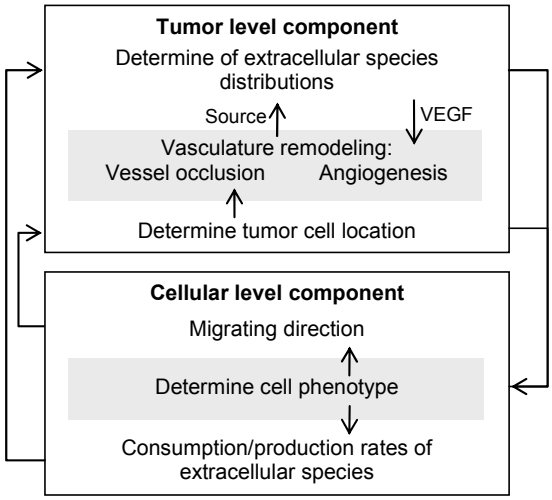

Fig. 1. Components of the model of brain tumor progression.

The location of tumor cells is determined by solving the following optimization problem:

$$\min z = w_1\sum_i d_{ii^T}^2 + w_2\sum_i\sum_{j>i}\frac{(2r_c - d_{ij})^2}{d_{ij}}u(2r_c - d_{ij}) + w_3\sum_i\sum_k\frac{(r_c + r_v - d_{ik})^2}{d_{ik}}u(r_c + r_v - r_{ik}), \tag{3}$$

where d_{ii^T}, d_{ij}, and d_{ik} are the distance between tumor cell i and its target position, tumor cell j and blood vessel k, respectively. r_c and r_v are the nominal radius of tumor cells and blood vessels, respectively. $u(\cdot)$ is the step function and $w's$ are constant weights. The target position for quiescent and proliferating cells is their current positions whereas the target position for the migrating cells is determined by their chemotaxis response and is computed as:

$$\mathbf{x}_i^T = \mathbf{x}_i^0 + a_i\mathbf{d}_i, \tag{4}$$

where $\mathbf{x}_i^0$ is the current position of migrating tumor cell i and $\mathbf{d}_i$ is the direction (unit) vector and a_i migrating distance. The direction vector is computed from a weighted sum of the oxygen and VEGF (as a surrogate of a chemorepellent) gradients. The migrating distance is derived from the individual tumor cell velocity, which is sampled from a normal distribution in accordance with experimental observations [29].

B. Cellular level model component

At the cellular level, tumor cell phenotype and migratory

behavior is determined by its local environment. Tumor cells require a minimum level of nutrients to thrive whereas the transduction of signaling cues regulates their phenotype (i.e., migratory or proliferative). It has been observed that the growth factor-induced phosphorylation of a downstream component of the MAPK signaling pathway (i.e., ERK) correlates with the migratory and proliferative behavior of tumor cells [30]. The MAPK signaling pathway can be triggered by several different growth factors, including TGFα. The cellular level model consists of a set of rules governing the behavior of tumor cells (Fig. 2). In brief, tumor cell phenotype depends on the activation level of the MAPK pathway and the availability of nutrients, whereas the migration direction depends on the response of migrating cells to chemical gradients. Furthermore, we assume that the tumor cells do not sense the chemotactic gradients with 100 % certainty. Thus we determine the migrating direction randomly from the half-space defined by the exact migrating direction and the perpendicular plane passing through the cell position as:

$$\mathbf{d}_i = \mathbf{d}_i^e + \mathbf{p}_i \,, \tag{5}$$

$$\mathbf{d}_i^e = \mathbf{g}_{i,o} + b\mathbf{g}_{i,v} \,, \tag{6}$$

where $\mathbf{d}_i^e$ and $\mathbf{d}_i$ are the exact and actual migrating directions, $\mathbf{p}_i$ is a random perturbation, $\mathbf{g}_{i,o}$ and $\mathbf{g}_{i,v}$ are the gradients of oxygen and VEGF at the location of migrating tumor cell *i* and *b* is a constant.

C. Effect of temozolomide on tumor cells

We use the data from the in vitro experiments of the effect of TMZ concentration on the proliferation of C6/lacZ cells [7] to estimate the killing rate as a function of the TMZ concentration. To determine the relation between TMZ concentration and the killing rate, we assume that the in vitro growth of both cell lines is described by the following system of ODEs [31]:

$$\begin{aligned} \frac{dp}{dt} &= k_1 q - k_2 p - \beta(C_{TMZ})\, p, \\ \frac{dq}{dt} &= 2k_2 p - k_1 q, \end{aligned} \tag{7}$$

where p and q are the number of proliferating and quiescent cells, respectively. k_1, k_2 and $\beta(C_{TMZ})$ are the transition rate from quiescent to proliferative, the mitosis rate and the killing rate as a function of the TMZ concentration, respectively. We use this two population model instead of the total population model to take into account that TMZ only affects proliferating cells. The parameters k_1 and k_2 where estimated [31] by fitting the model to experimental data [32] assuming a constant ratio of the proliferative to quiescent cells [33]. $\beta(C_{TMZ})$ is assumed to be a sigmoidal function (Gompertz function). The model (Eq. 7) was fitted to the data of the effect of TMZ on tumor cell proliferation to estimate the parameters of $\beta(C_{TMZ})$.

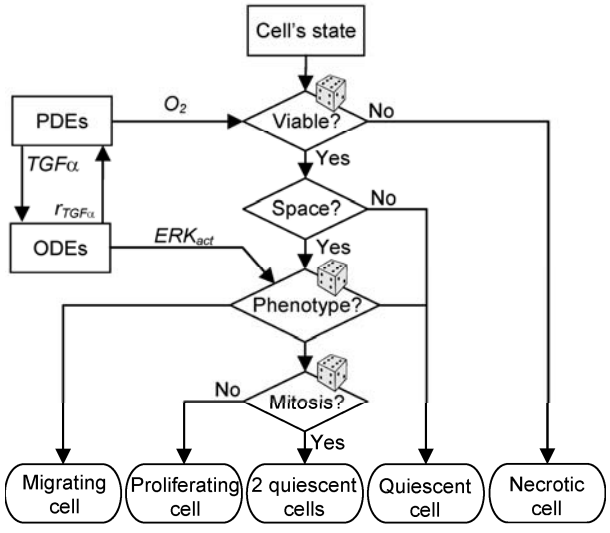

Fig. 2. Phenotype transitions tumor cells. Dice indicate stochastic processes.

III. Simulation Results

Kim *et al*., [7] evaluated the antitumor effect of different schedule-dose combinations of TMZ through in vivo orthotopic rat models of glioma. C6/lacZ tumor cells, a tumor rat-derived cell line that shows infiltrative growth in the brain (attc.org), were injected in to the white matter of Sprague-Dawly rats. The implanted tumors were treated with different schedule-dose combinations and the volume of the tumors was reported. We use the model to simulate the effect of TMZ on the progression of orthotopic models of glioma. Subsequently, we deploy the model to predict the outcome of alternative treatment strategies.

A. TMZ treatments of C6/lacZ tumors

We simulate the effect of three different schedule-dose combinations on the growth of C6/lacZ tumors. The schedule-dose combinations are given in Table I. Fig. 3 shows the experimental and predicted tumor volume at day 17 after implantation. As can be seen, the model predictions are in good quantitative agreement with the experimental data. Most importantly, the model is able to capture the relative efficacy of the different treatment modalities. Moreover, the simulations provide insights regarding the progression of the tumors.

Fig. 4 shows the time evolution of the treated tumors. At the early stages, the three treatments show a significant

TABLE I
SIMULATED TMZ TREATMENTS

Treatment	Schedule[a]	TMZ dose (mg/kg)
A0	Control	
A1	1:16	1
A2	1:16	2
A3	7:11	7

[a]Initial and last day of consecutive treatment since tumor implantation.

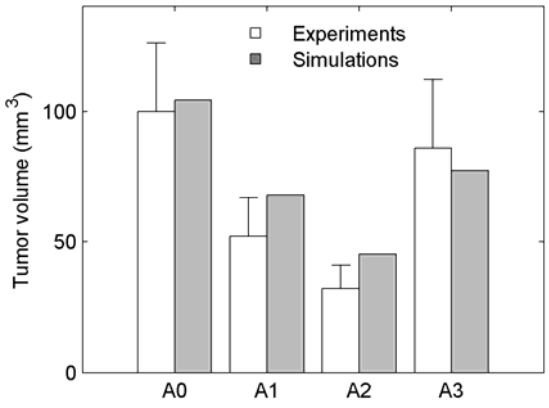

Fig. 3. Experimental and predicted volume of C6/lacZ tumors treated with TMZ. Experimental values represent the mean and the standard error [7]. A0 to A3 are the different treatments. See Table I for specifics.

retardation of tumor growth. However, the ratio of the volume of treated tumors to the untreated one eventually stabilizes for treatments A1 and A2. This result has a noteworthy implication if this trend would continuo for longer time. A simplified analysis, based on the observation that the simulated tumors approximately follow an exponential growth, a constant ratio of the volume of the treated to the untreated tumor, implies the following relationship between the growth rate constants:

$$\mu_{TMZ} = \mu_0 + \frac{1}{t}\ln a\,, \tag{8}$$

where μ_{TMZ} and μ_0 are the growth rate constants of the treated and untreated tumors and a is the constant volume ratio at later times. This relation (Eq. 8) suggests that as time increases the growth rate of the treated tumors approaches the growth rate of the untreated tumor regardless of the continuous administration of the drug at these concentrations.

B. Simulation of alternative treatments of TMZ

We deploy the model to simulate the outcome of alternative TMZ treatment strategies on C6/lacZ tumors. We test different schedule-dose combinations using the same amount of TMZ as treatment A3 and compare the tumor volume at day 17 from implantation. The test treatment strategies are given in Table II. The time progressions of the tumors under the different treatments are shown in Fig. 5. Of all the test treatments, C1 and C5 show a considerable improvement compared to treatment A3. Clearly, the main advantage of treatment C1 over A3 is the early administration of the drug. At early stages, tumor cells are exposed to higher concentrations of TMZ because the attraction to the vessels dominates the response to chemorepellent(s). Moreover, a larger fraction of the tumor cells are proliferating and therefore the tumor is more susceptible to TMZ. The effect of treatment C1 is a delay on the growth of the tumor. By day 17, the tumor under treatment C1 (Fig. 6) is very similar to the untreated tumor at day 12 (not shown).

TABLE II
SIMULATED TMZ TREATMENTS

Treatment	Schedule[a]	TMZ dose (mg/kg)
C1	1:5	7
C2	12:16	7
C3	3, 6, 9, 12, 15	7
C4[b]	7:11	7
C5[c]	7:11	3.5

[a]Initial and last day of consecutive treatment since tumor implantation.
[b]Simulation with no-angiogenesis.
[c]Two doses daily.

Treatments C2 and C3 produced tumors of similar volume than treatment A3. However, the morphology of the tumor under treatment C2 shows a different aspect (Fig. 6). The tumor has a decreased cellular density across the tumor rim expect at the inner side which is formed mainly by quiescent cells. However, the tumor probably would become similar to the tumor under A3 after the suspension of treatment.

Treatment C4 corresponds to the same schedule-dose than treatment A3 assuming that angiogenesis is completely blocked. Interestingly, blocking angiogenesis results in the

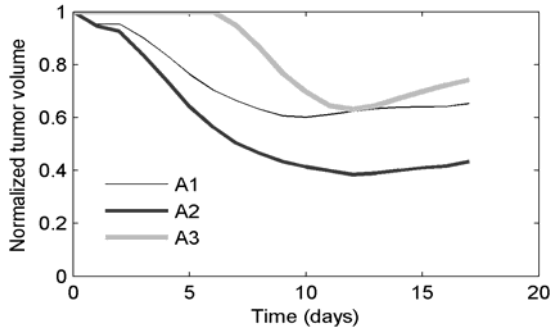

Fig. 4. Time progression of the C6/lacZ tumors treated with TMZ. The tumor volume is normalized with respect to the untreated tumor. See Table I for the specifics of treatments A1, A2 and A3.

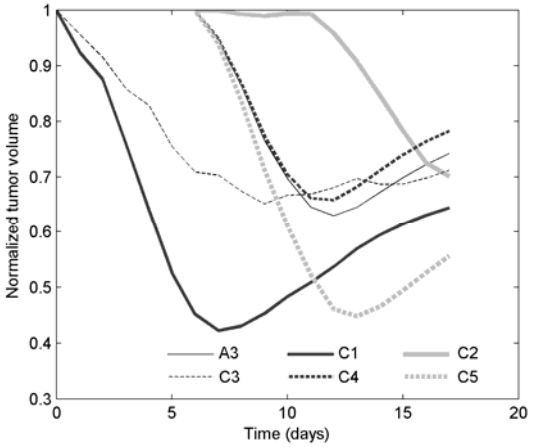

Fig. 5. Time progression of the C6/lacZ tumors treated with TMZ. The tumor volume is normalized with respect to the untreated tumor. See Table I for the specifics of treatment A3 and Table II for treatments C1 to C5.

largest volume of the test treatments. This is a consequence of the more marked chemotactic gradients pointing away from the tumor core, promoting the invasiveness of the tumor. In simulations where angiogenesis is allowed, newly

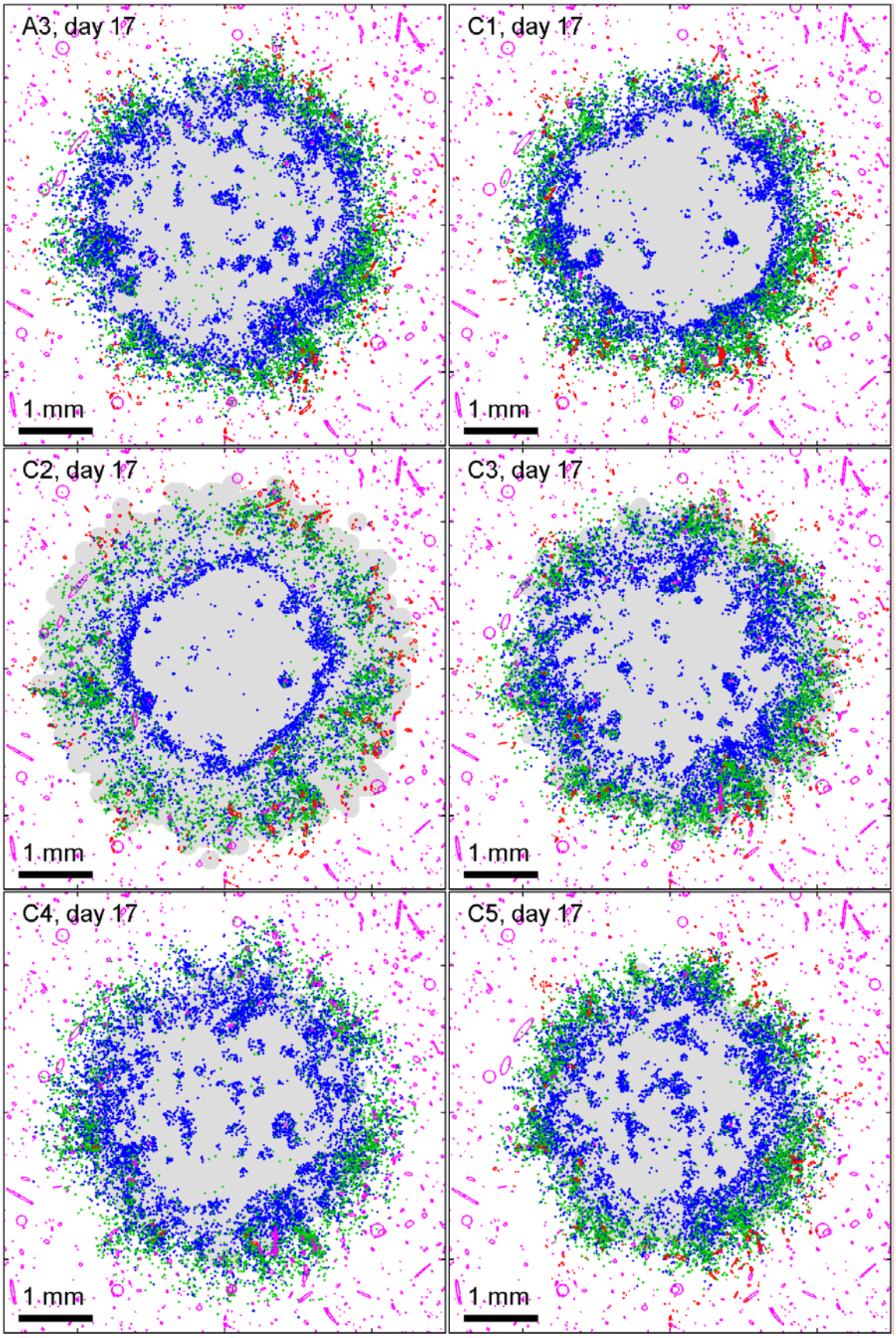

Fig. 6. Cross sections of C6/lacZ tumors under TMZ alternative treatments. Quiescent cells, migrating cells, pre-existing vessels and newly formed vessels are colored in blue, green, magenta and red respectively. Gray indicates the location where necrosis has occurred.

formed vessels attenuate the gradients of oxygen pointing outward the core of the tumor, retarding the invasive tumor cells.

IV. Discussion

Complementing standard procedures (i.e., surgery followed by radiotherapy) with TMZ treatment resulted in a statistically significant therapeutic benefit (an increase in median survival by 2.5 months) [6]. However, the overall outcome is still dismal. The limited effect of TMZ in tumor progression has been attributed in part to the development of tumor resistance to TMZ [7]. It is believed that several mechanisms may be responsible for tumor resistance to TMZ. One of the most accepted hypothesis proposes that the resistance is associated with increased levels of the enzyme O-6-methylguanin-DNA methyltransferase (MGMT), which repairs the DNA lesions induced by TMZ. Patients that had an increased level of inactivated MGMT had an improvement on the median survival of about 6 months [5]. Our simulation results suggest that the tumors may become resistant to TMZ by a different mechanism.

In our simulations of treatments of daily administration of TMZ, we observed that the ratio of the volume of the treated tumors to the untreated tumor stabilizes around a constant value depending on the TMZ dose. This implies that the growth rate (in terms of the volume of the tumor) of the treated tumor approaches the growth rate of the untreated tumor as time increases despite the persistent administration of TMZ. The mechanism of the resistance observed in our simulations depends on the response of the tumor cells to the harsh environment created by the collapse of the vasculature. The collapse of the vasculature is accompanied by an increase of tumor cells dwelling under hypoxia. These cells secrete a chemorepellent(s) that signals the tumor cells to flee from the hypoxic regions accelerating the expansion of the tumor. The balance of the promoting and inhibiting factors of tumor invasion resulted in the observed progression profiles in the simulations. The rate at which the growth rate of the treated tumors approaches the rate of the untreated one depends on the specific activity of TMZ against tumor cells. This specific activity can be increased by treatments targeting MGMT. According to these simulations, this would dampen the acceleration of the treated tumor but nevertheless the tumors would exhibit resistance to TMZ.

In attempts to increase the efficacy of TMZ, different treatment strategies are being explored. These studies are in general lengthy and resource consuming. Therefore, it is desirable to maximize the generation of insights from the results in order to design new studies. Mathematical modeling can be a powerful tool to improve the understanding of the complex interaction between the multiple factors affecting the outcome of the studies. Here we demonstrated that the proposed model of tumor progression is able to simulate the effect of different treatment strategies in orthotopic models of glioma tumors. Analysis of the simulations shed light on the possible mechanisms responsible for the observed experimental results and can help to design alternative treatment strategies and estimate the limitations of the treatment.

References

[1] M. Wrensch, Y. Minn, T. Chew, M. Bondy, and M. S. Berger, *Neuro Oncol*, vol. 4, pp. 278-99, 2002.
[2] A. Behin, K. Hoang-Xuan, A. F. Carpentier, and J. Y. Delattre, *Lancet*, vol. 361, pp. 323-331, 2003.
[3] L. M. DeAngelis, *N Engl J Med*, vol. 344, pp. 114-23, 2001.
[4] A. D. Norden and P. Y. Wen, *Neurologist*, vol. 12, pp. 279-292, 2006.
[5] J. L. Villano, T. E. Seery, and L. R. Bressler, *Cancer Chemother Pharmacol*, vol. 64, pp. 647-55, 2009.
[6] R. Stupp, et al., *New England Journal of Medicine*, vol. 352, pp. 987-996, 2005.
[7] J. T. Kim, et al., *Oncol Rep*, vol. 16, pp. 33-9, 2006.
[8] F. B. Furnari, et al., *Genes & Development*, vol. 21, pp. 2683-2710, 2007.
[9] M. Nakada, J. A. Niska, N. L. Tran, W. S. McDonough, and M. E. Berens, *Am J Pathol*, vol. 167, pp. 565-76, 2005.
[10] B. Salhia, N. L. Tran, M. Symons, J. A. Winkles, J. T. Rutka, and M. E. Berens, *Expert Rev Mol Diagn*, vol. 6, pp. 613-26, 2006.
[11] D. B. Hoelzinger, T. Demuth, and M. E. Berens, *Journal of the National Cancer Institute*, vol. 99, pp. 1583-1593, 2007.
[12] C. M. Park, et al., *Cancer Research*, vol. 66, pp. 8511-8519, 2006.
[13] H. B. Frieboes, X. Zheng, C. H. Sun, B. Tromberg, R. Gatenby, and V. Cristini, *Cancer Research*, vol. 66, pp. 1597-1604, 2006.
[14] R. P. Araujo and D. L. McElwain, *Bull Math Biol*, vol. 66, pp. 1039-91, 2004.
[15] N. Bellomo, N. K. Li, and P. K. Maini, *Mathematical Models and Methods in Applied Sciences*, vol. 18, pp. 593-646, 2008.
[16] H. M. Byrne, *Nature Reviews Cancer*, vol. 10, pp. 221-230, 2010.
[17] J. S. Lowengrub, et al., *Nonlinearity*, vol. 23, pp. R1-R91, 2010.
[18] K. A. Rejniak and L. J. McCawley, *Experimental Biology and Medicine*, vol. 235, pp. 411-423, 2010.
[19] A. R. A. Anderson and M. A. J. Chaplain, *Bulletin of Mathematical Biology*, vol. 60, pp. 857-899, 1998.
[20] N. V. Mantzaris, S. Webb, and H. G. Othmer, *Journal of Mathematical Biology*, vol. 49, pp. 111-187, 2004.
[21] A. A. Qutub, G. Liu, P. Vempati, and A. S. Popel, *Pac Symp Biocomput*, pp. 316-27, 2009.
[22] M. A. Chaplain, S. R. McDougall, and A. R. Anderson, *Annu Rev Biomed Eng*, vol. 8, pp. 233-57, 2006.
[23] A. Swierniak, M. Kimmel, and J. Smieja, *European Journal of Pharmacology*, vol. 625, pp. 108-121, 2009.
[24] T. S. Deisboeck, L. Zhang, J. Yoon, and J. Costa, *Nature Clinical Practice Oncology*, vol. 6, pp. 34-42, 2009.
[25] H. L. P. Harpold, E. C. Alvord, and K. R. Swanson, *Journal of Neuropathology and Experimental Neurology*, vol. 66, pp. 1-9, 2007.
[26] H. Hatzikirou, A. Deutsch, C. Schaller, M. Simon, and K. Swanson, *Mathematical Models & Methods in Applied Sciences*, vol. 15, pp. 1779-1794, 2005.
[27] K. R. Swanson, C. Bridge, J. D. Murray, and E. C. Alvord, Jr., *J Neurol Sci*, vol. 216, pp. 1-10, 2003.
[28] P. Tracqui, Reports on Progress in Physics, vol. 72, 2009.
[29] T. Demuth, et al., *Clinical & Experimental Metastasis*, vol. 18, pp. 589-597, 2001.
[30] C. R. Lind, et al., *Neuroscience*, vol. 141, pp. 1925-33, 2006.
[31] T. L. Siskind, "Modeling the effect of temozolomide on brain tumor growth. ," in *Departments of Chemical Engineering.* , vol. Baccalaureate degree. State College, PA Pennsylvania State University, 2010.
[32] X. X. Tian, Y. G. Zhang, J. Du, W. G. Fang, H. K. Ng, and J. Zheng, *Neuropathology*, vol. 26, pp. 178-87, 2006.
[33] H. C. Ugur, et al., *J Neurooncol*, vol. 83, pp. 267-75, 2007.